Subsurface channeling of keV ions between graphene layers: Molecular dynamics simulation

Yudi Rosandi,[1,2] Maureen L. Nietiadi,[1] and Herbert M. Urbassek[1,*]

[1]*Fachbereich Physik und Forschungszentrum OPTIMAS, Universität Kaiserslautern, Erwin-Schrödinger-Straße, D-67663 Kaiserslautern, Germany*

[2]*Department of Physics, Universitas Padjadjaran, Jatinangor, Sumedang 45363, Indonesia*

(Received 3 October 2014; revised manuscript received 23 February 2015; published 31 March 2015)

Using molecular dynamics simulation, we study the impact of 3 keV Xe ions at glancing incidence on a β-SiC (111) surface covered by graphene. On top of a full graphene layer covering the substrate, we add a graphene half-layer; the step forming where the half-layer terminates allows the entrance of glancing-incidence ions into a subsurface channel between graphene layers. We find a high channeling probability which leads to only little sputtering and damage formation. Typically, vacancy defects are formed at periodic intervals when the ion hits the uppermost graphene layer from below. Extended damage occurs when the ion hits the step edge itself. There we find several kinds of defects varying from adatoms over the formation of sp^1-bonded chains to hillocks.

DOI: 10.1103/PhysRevB.91.125441 PACS number(s): 79.20.Rf, 61.80.Jh, 79.20.Ap

I. INTRODUCTION

Ion irradiation of nanostructured and "two-dimensional systems" has recently gained interest. In their review [1] Krasheninnikov and Nordlund give an overview of recent research which concentrated in particular on carbon systems such as nanotubes and graphene layers. In [2] an overview of the defects induced in graphene by perpendicular ion impact is given. However, particularly interesting features appear under glancing ion incidence. Thus, recently Michely and co-workers studied ion impact on a graphene layer covering a metal—the Ir (111) surface—both by experiment and computer simulation; and highlighted interface channeling, defect formation, and ion trapping [3]. Further simulations studied ion impact on SiC covered by a graphene layer and discussed the differences between subsurface channeling in the substrate and interface channeling between the substrate and the graphene cover layer [4].

Glancing ion incidence on metals has been studied in considerably greater detail, both by experiment and by simulation [5–11]. Such glancing impact gives rise to the phenomenon of subsurface channeling where the projectile is channeled immediately under the surface. In this channeling mode the ion creates characteristic damage, such as vacancy islands aligned with the ion incidence direction (projected onto the surface) and even nanogrooves. This ample body of evidence for metallic targets is supplemented by more scarce studies of semiconductors [12,13] and ionic surfaces [14].

Several simulation studies have been published that analyzed the defects formed in two-dimensional carbon structures under ion impact. Electron irradiation of graphene produces isolated defects such as single vacancies or adatom-vacancy pairs [15]. Ion irradiation of carbon nanotube bundles was found to create intertube links which correspond to a change of sp^2 to sp^3 bonding [16]. The ion irradiation of two-shell (onionlike) fullerene structures was studied by DFT-based tight-binding simulations; again the creation of regions with sp^3-bonding characteristics was observed [17]. Ion irradiation of graphite also gives rise to the formation of sp^1- and sp^3-bonding defects [18,19]. Reference [1] gives an overview of radiation damage created in nanostructured carbon materials.

In the present paper we study glancing ion incidence on a SiC substrate covered by a multilayer (more precisely: one and a half layer) graphene sheet. Epitaxial graphene on SiC is easily synthesized and has been much studied due to its promising electronic properties [20,21]. The extra half layer of graphene on the substrate creates a surface step between the graphene layers which allows easy entrance for glancing ions in the subsurface graphene channel. Besides the channeling probabilities of such a system, we study the consequences of ion irradiation, viz. surface damage and sputtering.

II. METHOD

The target consists of a β-SiC substrate with a (111) Si-terminated surface; on top of it we place one full and one half-layer of graphene, see Fig. 1. β-SiC is also known as 3C-SiC; it has a cubic zincblende structure. Details of the structure are given in [4]. In short, the SiC crystallite consists of 18 SiC (111) layers and has a thickness of 42.5 Å. The area of the target surface amounts to 154×107 Å^2. A full graphene sheet is put on top of it with a lattice parameter of 2.46 Å; the nearest-neighbor distance amounts to 1.42 Å. Another half-layer of graphene is set on top of it, see Fig. 1.

The silicon atoms and substrate carbon atoms interactions are modeled by the Tersoff potential [22,23]. The high-energy region is splined to the Ziegler-Biersack-Littmark (ZBL) repulsive potential [24,25]. The interaction of carbon atoms in the graphene layers is modeled by the AIREBO potential without torsion term [26]. The interaction between graphene and the substrate is modeled by two Lennard-Jones potentials, one for the C and one for the Si atoms of SiC, with different σ and ϵ parameters. Between graphene and the substrate C atoms, the same parameters as in the van der Waals interaction in AIREBO are used: $\sigma_{\text{Gr-C}} = 3.4$ Å, and $\epsilon_{\text{Gr-C}} = 2.8$ meV. The interaction of graphene with the substrate Si atoms is fitted to the surface binding energy of 0.34 eV/(graphene unit cell) and the interlayer distance to the Si-terminated surface of $\Delta h = 2.58$ Å as calculated by DFT [27]. This gives us $\sigma_{\text{Gr-Si}} = 2.65$ Å and $\epsilon_{\text{Gr-Si}} = 0.117$ eV. The corrugation of the

*urbassek@rhrk.uni-kl.de; http://www.physik.uni-kl.de/urbassek/

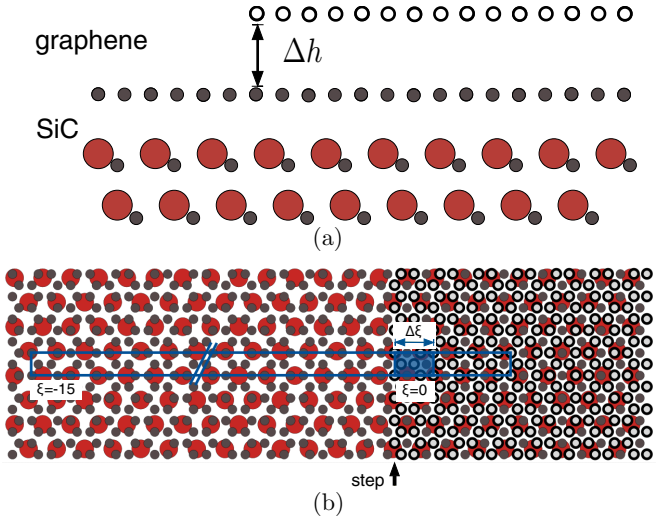

FIG. 1. (Color online) Sketch of the target surface, showing (a) top view and (b) side view. Brown circles show the uppermost Si atoms of the Si-terminated SiC (111) substrate. Full black circles denote C atoms of the fist graphene layer; open black circles denote C atoms of the second half-layer. The C atoms of the SiC substrate are not shown. The impact area is outlined with blue borders. $\Delta h = 3.354$ Å is the graphene interlayer distance.

graphene layer is negligible, 0.03 Å. The graphene interlayer distance amounts to $\Delta h = 3.354$ Å.

Before starting the bombardment simulation the system is relaxed to zero pressure and temperature by applying damping boundary conditions on the lateral sides of the target. The graphene surface is left free, while the bottommost substrate layer is kept fixed. These boundary conditions are also used during the simulation. These conditions are analogous to those used by us in previous surface channeling simulations [12,28].

As projectiles, we use Xe^+ ions with an impact energy of 3 keV. A previous study [4] showed that these massive ions give rise to more pronounced damage and channeling patterns than lighter Ar^+ ions. The ion incidence angle is fixed to 83° towards the surface normal. This is the minimum angle at which the ion is reflected from a SiC substrate covered by a full graphene layer, inducing neither damage nor sputtering in the target. At smaller angles, the ion will also damage a perfect graphene sheet; at larger angles, the ion will impart less energy to the target and damage formation will be reduced. Due to the wide channel width and the fact that we assume the electron density to be small in the channel, we disregard electronic stopping. Ions impact in the impact zone shown in Fig. 1. It is built on a unit surface mesh of width $\Delta\xi = 4.29$ Å and breadth $\Delta\eta = 2.47$ Å. The impact zone consists of 15 meshes in front of the step and 2 meshes behind the step. 20 impact points are chosen randomly inside each surface mesh, such that the total number of ion impacts simulated amounts to 340. We follow the trajectories up to 25 ps simulation time.

We analyze the damage created in the graphene layers by calculating the coordination number of each atom after irradiation. It is determined as the number of C neighbors of the atom within a sphere of radius $r_c = 1.8$ Å; this value is chosen in between the distance of nearest neighbors (1.42 Å) and second-nearest neighbors (2.46 Å) in graphene. Note that unstrained sp^3 bonds such as in diamond have a length of 1.54 Å, much less than r_c. In an intact graphene sheet, all atoms have three nearest neighbors (sp^2-bonded atoms). We shall call atoms with two—or fewer—nearest neighbors *undercoordinated* atoms; they will typically be bonded by sp^1 bonds. Atoms with four nearest neighbors will be denoted as *overcoordinated* atoms, bonded by sp^3 bonds.

The coordination numbers are calculated at the end of the impact simulation, at 3 ps after ion impact. For several selected events we analyzed the defect structures further by slowly quenching them within 25 ps to 0 K. The differences observed are minor, of the order of only 3%; we therefore presume that we can take our analysis of the as-irradiated samples to describe the trends of damage formation correctly.

III. RESULTS

A. Sputtering

3 keV Xe^+ ions impinging at 83° on a flat graphene sheet are reflected from it, inducing neither damage nor sputtering in the surface. However, when these ions impinge in the vicinity of a surface step in the graphene cover, abundant sputtering may result. Only graphene is sputtered; we found no Si or C atoms from the SiC substrate among the sputtered flux.

We display in Fig. 2 the sputter yield as a function of the distance ξ of the ion impact point from the step edge. We calculate this distance on the height of the upper graphene half-plane, such that the step edge itself is situated at $\xi = 0$. The figure shows a clear bimodal distribution. One maximum is at $\xi = 0$; it is due to ions colliding with step-edge atoms ("direct-hit" events). The second maximum at $\xi \cong -40$ Å is due to ions that are reflected from the lower graphene sheet and then hit the step edge from below ("indirect-hit" events). The distance of the indirect-hit impact points to the step edge can be estimated by a simple geometric model [8,29] as

$$x_c = 2\Delta h \tan\vartheta, \tag{1}$$

where $\Delta h = 3.354$ Å is the graphene interlayer distance, and $\vartheta = 83°$ is the ion incidence angle. This model gives $x_c = 55$ Å and denotes the outermost incidence points that can still

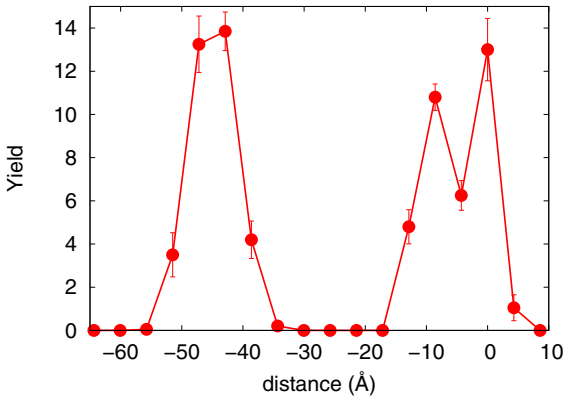

FIG. 2. (Color online) Sputter yield of a 3 keV Xe^+ ion impinging at 83° on a graphene-covered SiC crystal as a function of the ion impact point ξ in front of the step. Only C atoms originating from the graphene cover are sputtered.

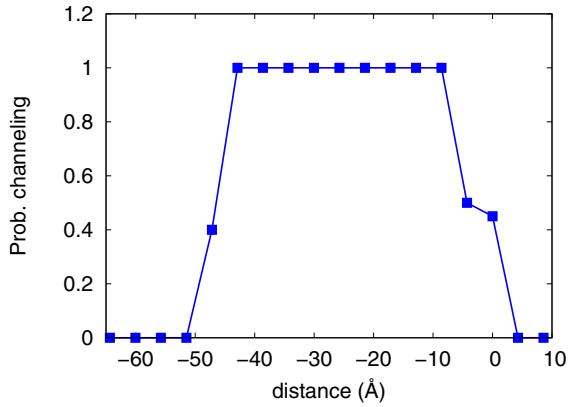

FIG. 3. (Color online) Channeling probability of 3 keV Xe^+ ions impinging at 83° on a graphene-covered SiC crystal as a function of the ion impact point ξ in front of the step.

induce sputtering. Indeed our simulation results (Fig. 2) agree nicely with this estimate. However, the maximum sputter yield in the simulation is found at slightly smaller distances from the step edge, since for such impacts the interaction with the upper half-layer of graphene is stronger.

B. Subsurface channeling

The dip found in the sputter yield (Fig. 2) between the two maxima is due to ions entering the channel between the upper and lower graphene layers. Such subsurface channeling events lead to little energy transfer to the substrate and to vanishing sputtering. Figure 3 demonstrates that indeed the probability for channeling is 100% for ion impacts between 43 and 9 Å in front of the step edge. For this quantitative evaluation we define an ion to be channeled if it performs at least two oscillations between the graphene sheets. In agreement with the geometrical model described above, the numerical value of the oscillation wavelength λ can be estimated to be equal to x_c. This criterion is more restrictive than that used in earlier work for subsurface channeling in Si, Pt, and SiC/graphene interfaces [4,5,12], where only one or half an oscillation inside the channel was required. Qualitatively, the high channeling fraction is not astonishing since graphene sheets have a high cohesive energy and therefore the ion does not easily break through them. Quantitatively, the efficiency of channeling can be assessed using Lindhard's critical angle ψ_2 [30]. It is calculated from the atomic numbers of projectile and target atom, Z_1 and Z_2, the projectile energy E, and the interatomic distance along the atomic string d via

$$\psi_2 = \left(\frac{3 Z_1 Z_2 e^2}{4\pi\epsilon_0} \frac{a^2}{d^3 E} \right)^{1/4}. \qquad (2)$$

Here $a = 0.8853 a_0/(Z_1^{2/3} + Z_2^{2/3})^{1/2}$ denotes the Thomas-Fermi screening radius and a_0 is Bohr's radius. The atomic distance along the ion flight direction is not unique, and may assume values of 1.42 and 2.46 Å; when assuming the average value, $d = 1.94$ Å, the critical angle amounts to 17.1°. However, for the larger interatomic distance of 2.46 Å—which spans the diagonal of the graphene hexagons—$\psi_2 = 14.3°$ and hence larger than the ion incidence angle with respect to the graphene plane.

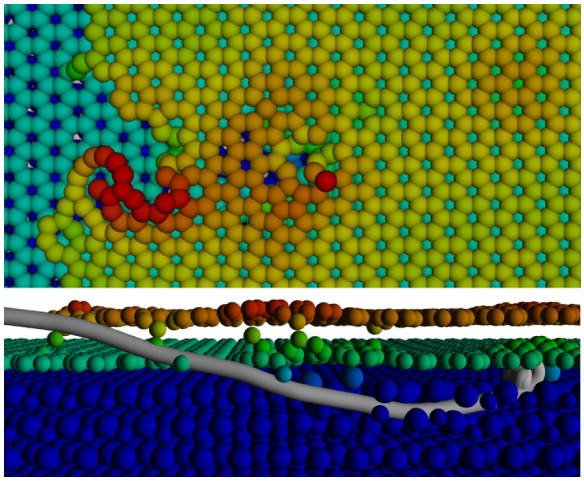

FIG. 4. (Color online) Top and side view of a direct-hit event. Colors indicate height above the substrate. The projectile trajectory is indicated in silver.

We conclude that the channel between the graphene layers allows for large critical angles and therefore supports channeling motion well.

C. Trajectories and energy loss

The fate of the ion—direct or indirect hit, channeling—has been discussed up to now using the sputter yield and the channeling probability as quantitative estimators. Figure 4 visualizes the trajectory of the ion and the damage created for a direct-hit event. In this particular case, the projectile is deflected downward by the encounter with the step edge atoms, penetrates the lower graphene layer, and is implanted in the substrate. At the collision place, the step edge is destroyed and a large vacancy island is formed immediately at the step edge. As a compensation, an adatom island has been created on top of the upper graphene layer. Such strong damage at the step edge is typical of direct-hit events also in metals [29]. The positions, where the ion penetrates the lower graphene layer and where it is buried in the vicinity of the substrate surface, are visible as small hillocks in the final damage structure.

Figure 5 visualizes an indirect-hit event. Here the damage is restricted to the step edge itself, since the ion is on its way away from the surface, such that further interactions do not occur. In particular, since the ion is not implanted, no second hillock structure is formed

Finally, Fig. 6 shows a channeled trajectory. The periodic motion of the ion gives rise to an equally periodic defect pattern; these defects are formed at the places where the projectile knocks from below on the upper layer. In the case shown, the defects can be characterized as small vacancy clusters consisting of two or three vacancies.

Sometimes we also find hyperchanneling trajectories, such as that shown in Fig. 7. As a rule the surface shows no defects for such events. Occasionally we observed the formation of five to seven defects at places where the projectiles knocks from below on the upper layer; such a case is highlighted in Fig. 7. In

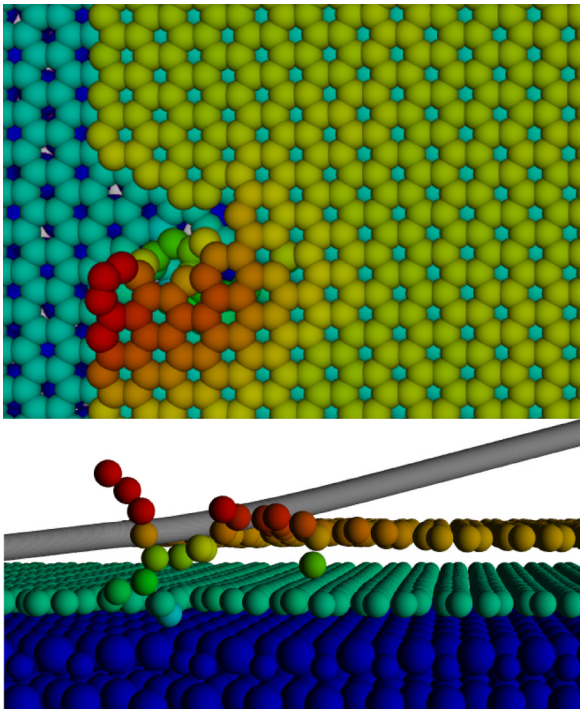

FIG. 5. (Color online) Top and side view of an indirect-hit event. Colors indicate height above the substrate. The projectile trajectory is indicated in silver.

these defects, the periodic arrangement of hexagons is broken up by the creation of an adjacent pentagon-heptagon pair; such defects have been reported earlier under ion or electron irradiation of two-dimensional carbon materials, especially nanotubes, under conditions where only isolated defects are formed [1]. In Fig. 7, only part of the entire simulation volume is shown; the channeling motion continues throughout the rest of the simulation volume without change and is therefore not included in the plot. The channeling motion shows a very regular oscillatory motion; its wavelength corresponds to 41 Å, in good agreement with our estimate of $\lambda = 55$ Å.

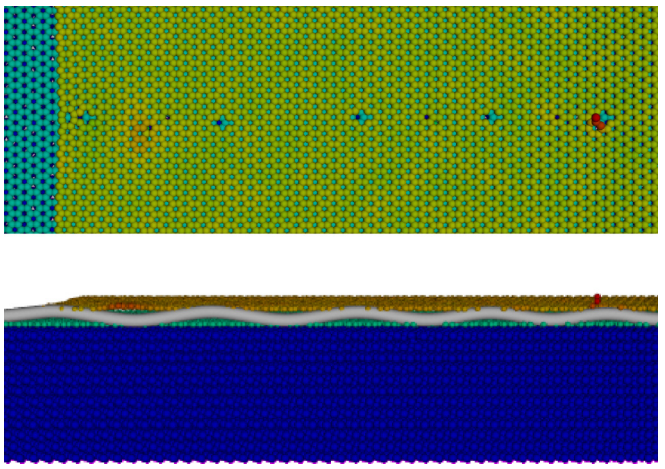

FIG. 6. (Color online) Top and side view of a channeling event. Colors indicate height above the substrate. The projectile trajectory is indicated in silver.

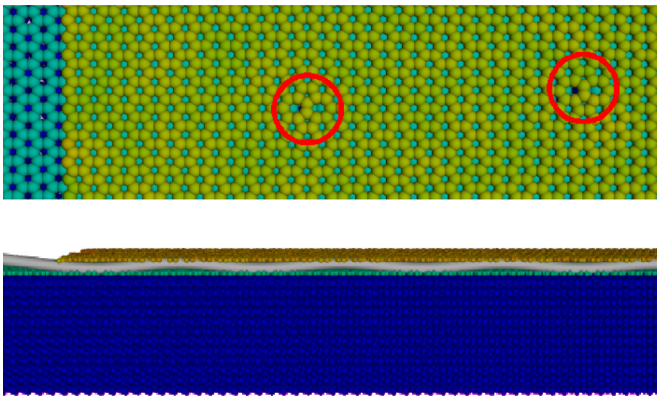

FIG. 7. (Color online) Top and side view of a hyperchanneling event. Colors indicate height above the substrate. The projectile trajectory is indicated in silver. The creation of two 5–7 defects has been marked.

In Fig. 8 we display the evolution of the projectile kinetic energy with path length traveled. Its derivative gives us the stopping force dE/dx. The energy lost is put mainly into damage creation in the target. The direct-hit case Fig. 8(a)

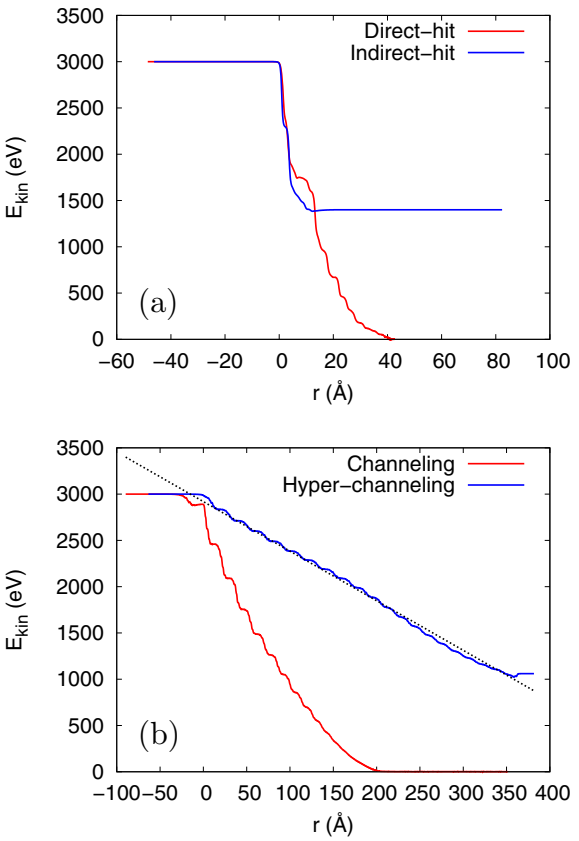

FIG. 8. (Color online) Evolution of the projectile kinetic energy as function of the path length traveled. $r = 0$ indicates the ion position immediately above the step edge. (a) Direct-hit and indirect-hit events shown in Figs. 4 and 5, respectively. (b) Channeling and hyperchanneled events shown in Figs. 6 and 7, respectively. The dashed line is a fit assuming a constant energy loss to $dE/dx = 5.73$ eV/Å.

shows that during the direct hit event, around 1 keV energy is lost; the remaining energy is delivered within the ensuing 20–30 Å that the projectile moves on, colliding with the lower graphene sheet and during implantation in the substrate.

The indirect-hit event displayed in Fig. 8(b) shows that the reflection of the projectile from the lower graphene layer costs only about 120 eV; the subsequent collision with the step edge costs somewhat more than 1 keV—in good agreement with the direct-hit case.

The energy loss curve of the channeled trajectories [Figs. 8(c) and 8(d)] is characterized by a sequence of steps indicating the losses upon colliding with the channel walls. Note the extended abscissa scale in these cases. In the hyperchanneled case [Fig. 8(d)] the energy loss in the channel is quite smooth and can be approximated by a constant energy loss of $dE/dx = 5.73$ eV/Å. The oscillations in the energy-loss curve reflect the ion motion in the channel. Whenever the ion hits the upper or lower graphene sheet, the energy steeply decreases by around 100 eV; in the channel itself energy loss is negligible. During each oscillation period of 41 Å the projectile suffers two collisions losing thereby around 200 eV; this estimate corresponds nicely to the measured energy loss of $dE/dx = 5.73$ eV/Å, cf. Fig. 8(d).

D. Damage creation

Figure 9 displays the number of defect atoms formed by 3 keV Xe ion impact at 83° incidence on the graphene surface as a function of the distance of the ion impact point from the step. The bimodal structure resembles closely that obtained for the sputter yield in Fig. 2; direct and indirect hits generate abundant damage while the damage under channeling conditions is minor. This appears plausible since both sputtering and damage formation require considerable local energy input into the surface. Since sputtering requires more energy, the absolute numbers of sputtered atoms are around a factor of 2 smaller than the number of damage atoms. Furthermore, we see that around 5 times more undercoordinated (sp^1-bonded) atoms are created than overcoordinated (sp^3-bonded) atoms. This can be rationalized by the fact that these defects are mostly created at the surface and hence undercoordination is more probable than overcoordination.

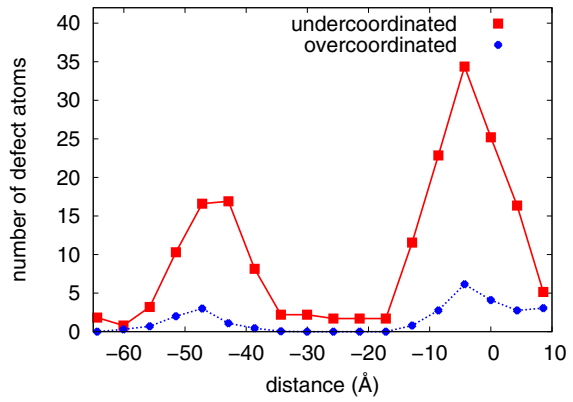

FIG. 9. (Color online) Average number of over- and undercoordinated defect atoms created by ion impact at a distance ξ from the step.

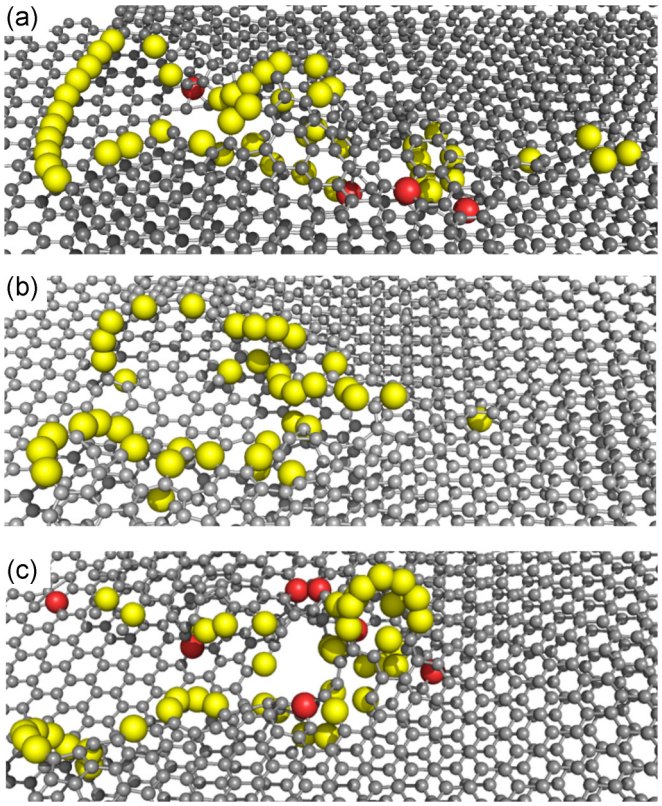

FIG. 10. (Color online) Perspective view of the surface showing defect formation close to the step edge. Colors denote coordination numbers and differentiate sp^1-bonded (yellow) and sp^3-bonded (red) defect atoms from ordinary sp^2-bonded atoms (gray). Defect atoms are emphasized by showing them by larger balls.

The nature of the defects can be analyzed further with the help of selected snapshots. Figure 10 shows several close-up views of the damage generated for nonchanneling events close to the step edge; in all these cases direct-hit events are shown. The sp^2 bonds characterizing graphene have been destroyed near the impact point, in particular in the upper graphene layer. The majority of defects formed are undercoordinated and decorate the rims of the hole formed in the upper graphene sheet. As a prominent feature, sp^1-bonded C chains have formed. Figure 10 shows an example of a chain consisting of 11 atoms. The chains may form loops on top of the upper plane [see Fig. 10(c)] or descend down towards the lower plane in front of the step edge [Fig. 10(a)]. Comparatively few overcoordinated defect atoms have been formed; many of these are found on adatom positions.

We found that occasionally the upper graphene layer stays intact and forms a buckling cover above the damage occurring underneath. A view of a buckled surface at some distance from the step edge is presented in Fig. 11. It shows a case where the ion has not hit the step edge but entered in between the two graphene layers. In this case, considerable damage has occurred in the interlayer region. While typically five times more under- than overcoordinated defects are created, in this particular case a considerable number of sp^3-bonded atoms have been generated and several bonds between the sheets have formed. Due to the debris accumulating between the sheets, the

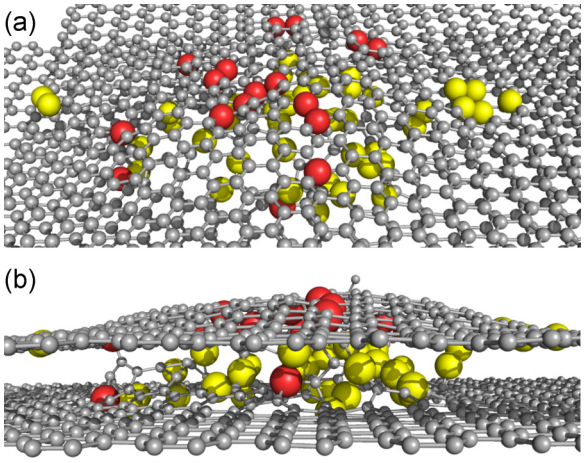

FIG. 11. (Color online) Perspective and side view showing buckling of the upper graphene layer after impact. Colors denote coordination numbers as in Fig. 10.

the upper layer is pushed upwards. The material between the graphene sheets looks strongly defective and even amorphous.

We note that the defect structures reported here were determined at the end of the impact simulation, at 3 ps after ion impact. When subjecting them to an anneal—10 ps at 1000 K—we found that some of the sp^1 chains displayed in Fig. 10 were not stable and decayed. In particular those chains reaching from the upper graphene sheet downward would disappear while the chains lying on the upper sheet survived. However, the total changes in the number of defect atoms were in the order of 5 at maximum showing that our analysis provides us with the correct trends of damage formation.

E. Surface waves

After ion impact surface waves are excited in the top graphene layer, consisting of transverse out-of-plane oscillations; this typically occurs under channeling conditions. The excitation of transverse waves by ion impact was previously reported by Smith *et al.* after impact of 250 eV fullerene onto graphite [31]. Figure 12 shows snapshots of one such event. A new wave crest is excited each time the channeled ion knocks at the top graphene layer; this leads to three distinct wave excitations in Fig. 12(c). The elastic wave runs sideways away from it. At a time of 0.67 ps after ion impact [Fig. 12(d)] the wave starts surpassing the projectile; later we see also wave propagation ahead of the projectile. The projectile has a speed of 3.8 (2.0) km/s at the time of the snapshots [Figs. 12(c) and 12(d)]; these velocities are evidently subsonic. The amplitudes observed are substantial and reach 4 Å for outward motion, but only 0.7 Å for motion toward the surface. The origin of the anisotropy is the very weak interaction between layers, which lets the upper graphene sheet separate from the surface.

We can calculate a wave speed from the distance covered by the wavefronts. Due to the multiple wave excitation this may not be done in the direction of the projectile, but transverse to it. From Fig. 12 we obtain a wave velocity of 4.5 ± 0.5 km/s.

For comparison we note that the transverse sound velocity with in-plane polarization in graphene amounts to 14 km/s [32]. The theory of transverse out-of-plane waves is more

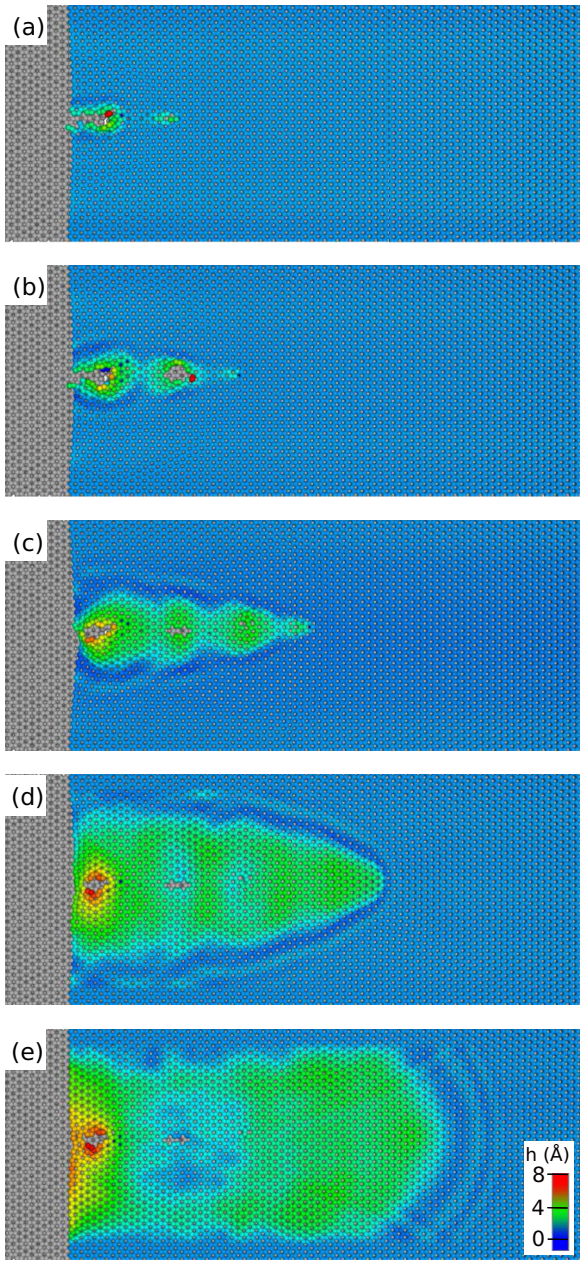

FIG. 12. (Color online) Top view snapshots showing the emergence of a surface wave in the graphene top layer, taken at 0.15, 0.23, 0.37, 0.67, and 1.20 ps after ion impact. Colors denote height above the substrate. The white point indicates the projectile.

complex [32,33]. If the interlayer interaction is ignored, these waves have a quadratic dispersion, such that a sound velocity cannot be properly defined; the quadratic term originates from the bending stiffness of graphene layers. The interlayer interaction adds a linear term to the dispersion; the linear term can be interpreted as sound with a velocity of $v_s = \sqrt{C_{44}/\rho}$, where C_{44} is the corresponding shear elastic modulus and $\rho = 2.25$ g/cm^3 is the mass density (here taken equal to that of graphite). Values for the elastic modulus C_{44} given in the literature show a large spread, with values ranging from 0.18–0.35 GPa to 5 GPa [32]; this gives sound velocities ranging from 0.34 to 1.5 km/s. These are all smaller than the

values obtained in our simulation. We conclude that for the short wavelengths considered here, the quadratic term in the dispersion law is essential.

IV. CONCLUSIONS

Our molecular dynamics simulations show that glancing-incidence keV ions may be easily channeled between graphene layers. The reason here is twofold: (i) The small interatomic distance d of C atoms within the graphene sheet causes a large critical angle for channeling [Eq. (2)]; and (ii) the large interplanar distance between graphene sheets, Δh, makes it easy for ions to enter the channel. In addition, the strong binding energy within the graphene sheets reduces dechanneling.

Ion impact close to the boundary of a second-layer graphene sheet has a number of consequences which may be easily recognizable in AFM experiments of ion-bombarded graphene targets.

(1) Ion impact on the step edge itself leads to strong damage, visible in the form of extended surface vacancy islands, and sp^1-bonded C atom chains. On average, approximately five times more undercoordinated (sp^1-bonded) defects than overcoordinated (sp^3-bonded) defects are formed.

(2) Subsurface channeling between the graphene layers gives rise to a chain of isolated defects in the upper graphene layer extending along the ion-beam direction over long distances (> 10 nm).

(3) Less well-channeled trajectories create surface buckling; this is due to defects forming in both graphene sheets, where sp^3-bonded C atoms are pushed in between the layers giving rise to surface buckling.

(4) Hyperchanneled trajectories will create no or only very small damage, such as five to seven defects.

(5) Due to the weak coupling between graphene layers, high-amplitude transverse waves in the graphene sheets are excited.

ACKNOWLEDGMENT

Y.R. acknowledges funding from the Indonesian Directorate General of Higher Education (DIKTI), Contract No. 1046/UN6.R/PL/2014.

[1] A. V. Krasheninnikov and K. Nordlund, J. Appl. Phys. **107**, 071301 (2010).
[2] O. Lehtinen, J. Kotakoski, A. V. Krasheninnikov, A. Tolvanen, K. Nordlund, and J. Keinonen, Phys. Rev. B **81**, 153401 (2010).
[3] S. Standop, O. Lehtinen, C. Herbig, G. Lewes-Malandrakis, F. Craes, J. Kotakoski, T. Michely, A. V. Krasheninnikov, and C. Busse, Nano Lett. **13**, 1948 (2013).
[4] Y. Rosandi and H. M. Urbassek, Nucl. Instrum. Method B **340**, 5 (2014).
[5] A. Redinger, H. Hansen, U. Linke, Y. Rosandi, H. M. Urbassek, and T. Michely, Phys. Rev. Lett. **96**, 106103 (2006).
[6] H. Hansen, A. Redinger, S. Messlinger, G. Stoian, Y. Rosandi, H. M. Urbassek, U. Linke, and T. Michely, Phys. Rev. B **73**, 235414 (2006).
[7] Y. Rosandi and H. M. Urbassek, Nucl. Instrum. Method B **256**, 373 (2007).
[8] A. Redinger, Y. Rosandi, H. M. Urbassek, and T. Michely, Phys. Rev. B **77**, 195436 (2008).
[9] A. Redinger, S. Standop, T. Michely, Y. Rosandi, and H. M. Urbassek, Phys. Rev. Lett. **104**, 075501 (2010).
[10] Y. Rosandi, A. Redinger, T. Michely, and H. M. Urbassek, Phys. Rev. B **82**, 125440 (2010).
[11] A. Redinger, S. Standop, Y. Rosandi, H. M. Urbassek, and T. Michely, New J. Phys. **13**, 013002 (2011).
[12] Y. Rosandi and H. M. Urbassek, Phys. Rev. B **85**, 155430 (2012).
[13] Y. Rosandi and H. M. Urbassek, Surf. Sci. **615**, 41 (2013).
[14] F. Krok, S. R. Saeed, Z. Postawa, and M. Szymonski, Phys. Rev. B **79**, 235432 (2009).
[15] M. Yamamoto, Y. Asayama, M. Yasuda, H. Kawata, and Y. Hirai, J. Vacuum Sci. Technol. B **32**, 06FK01 (2014).
[16] E. Salonen, A. V. Krasheninnikov, and K. Nordlund, Nucl. Instrum. Methods Phys. Res. Sect. B **193**, 603 (2002).
[17] R. Astala, M. Kaukonen, R. M. Nieminen, G. Jungnickel, and T. Frauenheim, Phys. Rev. B **63**, 081402 (2001).
[18] M. Henkel and H. M. Urbassek, Nucl. Instrum. Method B **145**, 503 (1998).
[19] R. Smith, C. Nock, S. D. Kenny, J. J. Belbruno, M. Di Vece, S. Palomba, and R. E. Palmer, Phys. Rev. B **73**, 125429 (2006).
[20] M. Ruan, Y. Hu, Z. Guo, R. Dong, J. Palmer, J. Hankinson, C. Berger, and W. A. de Heer, MRS Bull. **37**, 1138 (2012).
[21] L. O. Nyakiti, V. D. Wheeler, N. Y. Garces, R. L. Myers-Ward, J. C. R. Eddy, and D. K. Gaskill, MRS Bull. **37**, 1149 (2012).
[22] J. Tersoff, Phys. Rev. B **39**, 5566 (1989).
[23] R. Devanathan, T. Diaz de la Rubia, and W. J. Weber, J. Nucl. Mater. **253**, 47 (1998).
[24] J. F. Ziegler, J. P. Biersack, and U. Littmark, *The Stopping and Range of Ions in Solids* (Pergamon, New York, 1985).
[25] H. Hensel and H. M. Urbassek, Nucl. Instrum. Method B **142**, 287 (1998).
[26] S. J. Stuart, A. B. Tutein, and J. A. Harrison, J. Chem. Phys. **112**, 6472 (2000).
[27] A. Mattausch and O. Pankratov, Phys. Rev. Lett. **99**, 076802 (2007).
[28] H. M. Urbassek, C. Anders, and Y. Rosandi, Nucl. Instrum. Method B **269**, 947 (2011).
[29] A. Friedrich and H. M. Urbassek, Surf. Sci. **547**, 315 (2003).
[30] J. Lindhard, Mat. Fys. Medd. K. Dan. Vidensk. Selsk. **34**, 14 (1965).
[31] R. Smith, K. Beardmore, A. Gras-Marti, R. Kirchner, and R. P. Webb, Nucl. Instrum. Method B **102**, 211 (1995).
[32] P. Lambin, Appl. Sci. **4**, 282 (2014).
[33] H. Zabel, J. Phys.: Condens. Matter **13**, 7679 (2001).